Modeling Strategic Behaviors of Renewable-storage System in Low-inertia Power System

Kexin Li, *Student Member*, *IEEE*, Hongye Guo, *Member*, *IEEE*, Cheng Feng, *Member*, *IEEE*, Songtai Yu, and Yong Tang, *Senior Member*, *IEEE*

***Abstract*—In power systems with high proportion of variable renewable energy, the scarcity of inertia and primary frequency response (IPFR) becomes a critical issue. This evolution necessitates the emergence of corresponding markets. The increasing variety of markets and the diversity of market participants have led to more complex bidding behaviors than before, which need be thoroughly studied. This paper proposes a bi-level model to analyze the bidding behaviors of a renewable-storage system (RSS) acting as a price maker in multiple markets. The nonlinear relationship between IPFR and system frequency is modeled. To depict the characteristics of IPFR and future markets, the unit commitment (UC) process is embedded. To address the nonconvexity caused by the UC process in the proposed bi-level model, a solution approach based on penalty function and dual theory is presented. The proposed model and its solution method are applied to a case study based on the IEEE30-bus system and historical operational data from the California Independent System Operator. The case study results illustrate that the proposed model can effectively characterize the complex bidding behaviors of RSS in multiple markets and validate the efficacy of the solution method.**

***Index Terms*—Inertia, primary frequency response, renewable-storage, bidding behavior, unit commitment.**

Received: October 8, 2024
Accepted: May 22, 2025
Published Online: September 1, 2025

Kexin Li is with the Department of Electrical Engineering, Tsinghua University, Beijing 100084, China; and also with the China Electric Power Research Institute, Beijing 100192, China (e-mail: li-kx20@tsinghua.org.cn).

Hongye Guo (corresponding author) and Cheng Feng are with the Department of Electrical Engineering, Tsinghua University, Beijing 100084, China (e-mail: hyguo@tsinghua.edu.cn; fengc.2019@tsinghua.org.cn).

Songtai Yu is with the Beijing Power Exchange Center, Beijing 10003, China (e-mail: yust08@163.com).

Yong Tang is with the State Key Laboratory of Power Gird Safety (China Electric Power Research Institute), Beijing 100192, China (e-mail: tangyong@epri.sgcc. com.cn).

DOI: 10.23919/PCMP.2024.000200

NOMENCLATURE

A. Sets

Ω_{VRE}	set of variable renewable generators
Ω_{TH}	set of thermal generators
Ω_{es}	set of energy storage
Ω_{RSS}	set of renewable-storage

B. Variables

$x_{i,t,\omega}^{\mathrm{TH}}$	on/off status of thermal generator i
$\alpha_{i,b,t}^{\mathrm{EN}}$ (\$/MW)	generator i offering price of block b in energy market
$\alpha_{i,b,t}^{\mathrm{D/C}}$ (\$/MW)	energy storage i discharge/charge price of block b in energy market
$\alpha_{i,t}^{\mathrm{IN}}$ (\$/(MW·s/Hz))	generator i offering price in inertia market
$\alpha_{i,t}^{\mathrm{Re/PF}}$ (\$/MW)	generator i offering price in reserve market
$P_{i,b,t,\omega}^{\mathrm{G,EN}}$ (MW)	generator i cleared quantity in block b in energy market
$P_{i,b,t,\omega}^{\mathrm{D/C,EN}}$ (MW)	energy storage i cleared discharge/charge quantity in offering block b in energy market
$P_{i,b,t,\omega}^{\mathrm{RSS,PEN/NEN}}$ (MW)	renewable-storage i cleared discharge/charge capacity in offering block b in energy market
$H_{i,t,\omega}^{\mathrm{VI}} / H_{t,\omega}^{\mathrm{T0}}$ (MW·s/Hz)	virtual inertia provided by participant i/system total inertia
$P_{i,t,\omega}^{\mathrm{G,IN/PF}}$ (MW)	capacity of participant i to provide virtual inertia/PFR
$P_{i,t,\omega}^{\mathrm{Re}}$ (MW)	capacity of participant i to provide reserve
$\Delta P_{t,\omega}^{\mathrm{TH/RE,TO}}$ (MW)	PFR from thermal generators/other sources

$E_{i,t,\omega}^{\mathrm{EN}}$ (MWh) energy storage i stored energy

$P_{i,t,\omega}^{\mathrm{W,EN/PF/IN/Re}}$ (MW) capacity of VRE generator i in renewable-storage system providing energy/inertia/PFR/ reserve

$P_{i,t,\omega}^{\mathrm{RSS,D/C/PF/IN/Re}}$ (MW) energy storage unit in the ith renewable-storage system cleared discharge/charge/inertia/PFR/reserve quantity

$C_{t,\omega}^{\mathrm{U/D\text{-}TO}}$ ($) system total start-up and shut-down cost

$C_{t,\omega}^{\mathrm{EN/IPFR/Re}}$ ($) system costs in energy/IPFR/reserve market

R^{RSS} ($) RSS total profits in multi-market

$R_{\omega}^{\mathrm{EN/IPFR/Re}}$ ($) RSS profits from energy/IPFR/ reserve market in scenario

$\lambda / \mu / \rho / \sigma / \phi / \psi$ dual variables of corresponding constraint

C. Parameters

ΔD (MW) system disturbance

π_{ω} probability of scenario ω in the market

$C_i^{\mathrm{P,Op}}$ ($/MWh) cost of generator/storage i providing energy

$\alpha_{i,b}^{\mathrm{min/max}}$ ($/MW) upper and lower caps of the offering price for block b of generator i

$T_{\mathrm{PFR}}^{\mathrm{TH/VI}}$ (s) delivery time of thermal generators/other resources providing PFR

H_i^{TH0} (MW·s/Hz) inertia provided by thermal generator i

$P_i^{\mathrm{G,Min/Max}}$ (MW) lower/upper cap of available capacity in generator i

P_i^{Ramp} (MW) thermal generator i ramp capacity

$K_i^{\mathrm{U/D}}$ ($) thermal generator i up/down cost

$T_i^{\mathrm{U/D}}$ the minimum up/down time of thermal generator i

$P_{t,\omega}^{\mathrm{Re\text{-}min}}$ (MW) system reserve requirement

ζ_t (%) reserve deployment factor at time t

$C_i^{\mathrm{H,Op}}$ ($/(MW·s/Hz)) cost of generator/storage i providing inertia

N_{T} number of time periods

E_i^{Initial} (MWh) energy storage i initial stored energy

M large positive constant

$D_{t,\omega}$ (MW) system demand at time t in scenario

$\Delta f_{\max}$ (Hz) maximum system quasi-steady-state frequency deviation

$C_{i,t,\omega}^{\mathrm{D/U}}$ ($) thermal generator i shut-down/ start-up cost at time t scenario ω

$E_i^{\mathrm{EN_{max}}}$ (MWh) energy storage i maximum capacity

$P_{i,t,\omega}^{\mathrm{WTMAX}}$ (MW) maximum available capacity of VRE generator i in RSS

$P_{i,t,\omega}^{\mathrm{CTMAX/DTMAX}}$ (MW) maximum discharge and charge capacity of storage i in RSS

η_i charging or discharging efficiency of storage i

$F_{\mathrm{RoCoF\text{-}max}}$ (Hz/s) maximum rate of change of frequency

$P_i^{\mathrm{G,PF0}}$ (MW) primary frequency response provided by thermal generator i

I. Introduction

To address potential problems caused by climate change, many countries have formulated energy transition strategies. In the process of meeting their objectives, the role of variable renewable energy (VRE) is increasingly important in power system [1], [2]. International Energy Agency indicates that VRE will become the predominant power source in 2027, accounting for 38% of the global power generation at that time [3].

With the increasing proportion of VRE in power systems, conventional fossil-based generators have been gradually replaced. For example, Pennsylvania, New Jersey, Maryland Interconnection LLC (PJM) indicates that 35 000 MW of coal-fired generators have retired in the recent decades, accounting for 81% of the total retired generation [4]. However, many problems appear with the retirement of conventional fossil generators, such as the deficiency of inertia and primary frequency response (IPFR) in power systems [5]. The lack of the corresponding resources affects the resilience of power systems, resulting in sharper frequency drops after disturbances [6].

Many system operators have been aware of the potential problems caused by the shortage of IPFR resources and have implemented many strategies to handle low-inertia problems. For example, Finland power system operator has implemented a new product named fast frequency reserve (FFR), whose response speed (within 1.3 s) is faster than traditional frequency response products (7.5 s) [7], [8]. In the United Kingdom, National Grid Electricity System Operator has procured 12.5 GVA·s of inertia from five parties through a six-year contract [9].

To hedge the variability of VRE, energy storage (ES) has also been widely introduced into power systems [10] [11]. For instance, PJM stated that the colocation of

storage with renewable resources has become a trend within its dispatch area [4]. The report shows that an additional 131 MW of co-located storage is planned to be online between 2023 and 2024 in PJM, accounting for 69% of the total planned storage [12]. Due to its ability to smooth out the variable generation of VRE, ES has operated with VRE in many cases.

With the increasing capacity of VRE and ES and the growing demand for extra IPFR in low-inertia power systems, many studies have explored the ability of VRE and ES to provide IPFR. In [13]–[15], VRE and ES provide IPFR by working in de-rated mode instead of their normal working mode, i.e., maximum power point tracking (MPPT). In the de-rated mode, VRE generators and ES reserve a portion of the available capacity to provide IPFR when a disturbance occurs. Further, some studies work on the power system operation, considering their ability to provide IFPR. Reference [16] develops a stochastic unit commitment (SUC) model, which considers both thermal generators and ES to provide frequency support. Reference [17] proposes a system scheduling model in which wind turbines can be controlled to provide virtual inertia and primary frequency response.

Studies have also designed IPFR market mechanisms to quantify the monetary value of IPFR. Reference [18] designs an inertia and frequency response market mechanism. However, the ability of VRE to provide IPFR has been ignored. In [19], an inertia market clearing mechanism is proposed in which various types of generators, including VRE, can provide inertia. Reference [20] develops a pricing scheme for wind turbines and fossil-based generators providing IPFR services. However, in [19] and [20], the prices are determined by the shadow prices generated from the market clearing process, where bidding for IPFR is not allowed. This limitation weakens the participants' initiative to provide inertia services. Reference [21] proposes an IPFR market mechanism that allows various types of generators to provide IPFR and bid to demonstrate IPFR prices. However, the above studies focus mainly on the clearing process while ignoring the strategic bidding behaviors of participants when facing various kinds of categories in power markets.

To improve IPFR market mechanism design for future power systems, it is better to simulate and clarify the bidding behaviors of various participants. Considering that it has become a trend for VRE stations to be equipped with ES, renewable-storage system (RSS) is chosen as the object of this paper to study the strategic bidding of market participants.

Many studies investigate the bidding strategies of RSSs, including wind-storage system (WSS) and photovoltaic-storage system (PSS) in energy and ancillary markets. Reference [22] proposes a risk-averse stochastic optimization model to determine the bidding strategy of WSS in energy markets. Reference [23] builds a robust optimization model to indicate the bidding behavior of PSS in the energy market, while [24] presents a predictive control based robust model to obtain the optimal bidding strategies of the RSS in energy and regulation markets. References [25] and [26] obtain the bidding behavior of WSS in energy and ancillary markets by building a stochastic optimization model, in which the Monte Carlo and multi-stage scenario trees are used to generate various scenarios, respectively. In [27], a robust optimization model is developed considering wind uncertainty and financial risk to analyze WSS bidding strategies in energy and ancillary markets, whereas reference [28] proposes a mixed integer optimization model based on demand-supply curve methods and linear decision rules to analyze the bidding behaviors of WSS in energy and ancillary markets.

Although there are many studies on the bidding behaviors of RSS, it is still difficult to present and analyze their behaviors in future high-renewable-penetrated power markets because of three limitations. First, the current studies do not include IPFR process in the analysis of RSS bidding behavior. Studies in [22]–[28] are limited to energy and traditional ancillary markets. However, as IPFR is closely integrated with system operation [16], [21], it is crucial to consider IPFR to indicate RSS bidding behavior in future markets. Second, RSS is modeled as a price-taker in all markets in [22]–[27], or considered as price-takers in ancillary markets in studies [28]. This fails to apply in future power systems, as the effects of RSS bidding behavior on market clearing results will become more pronounced with the growth of VRE penetration. Thus, RSS should be modeled as a price-maker to analyze its complicated bidding behavior. Third, only economic dispatch (ED) has been modeled in bidding strategies analysis models, while the unit commitment (UC) process is ignored, rendering unsuitable for future power systems. The UC process should be considered as the volatility of VRE output will lead to changes in the on/off status of thermal generators during the day, and system IPFR is closely associated with generators' on/off status.

To overcome these limitations and capture the features of RSS strategic behavior in future markets, it is necessary to establish a bi-level bidding model, in which the lower level encompasses a market clearing model, including energy, IPFR, and the reserve market, and the upper level indicates the profits of the strategic RSS.

The contributions of this paper can be summarized as follows.

1) A novel bi-level bidding behavior model is proposed, which can demonstrate the bidding behaviors of a price-maker RSS in a comprehensive power market,

including energy, traditional ancillary services and IPFR.

2) A solution approach based on penalty function and dual theory is presented to address the non-convexity brought by the UC process in the bi-level model.

3) The proposed model and solution are tested through a case study based on historical operation data from California Independent System Operator (CAISO), demonstrating the complicated bidding behaviors of RSS in future power systems.

The rest of the paper is organized as follows. Section II describes the spot market structure in a high VRE penetration system and proposes the bi-level model framework. Section III indicates the bi-level model formulation. Section IV develops the solution of the proposed model. Section V illustrates the case study and analyzes the results. Finally, Section VI concludes the paper.

II. Problem Description

A. Spot Market Structure in a High VRE Penetration System

The current spot market mainly includes energy markets to meet demand requirements and reserve markets to ensure system security after a disturbance occurs.

With the replacement of thermal generators, system IPFR resources will become scarcity in future high VRE penetration systems [5]. IPFR acts before reserve services, which mainly affects the first 30 s after system disturbance occurrence. During this period, IPFR decreases the frequency decline rate and ensures that the frequency is affordable before reserve service is deployed [16], [19]. Thus, the IPFR market is necessary to incentivize various types of sources to provide IPFR.

IPFR can be provided by various types of sources. The VRE generator and ES offer IPFR by reserving a portion of the available capacity and operating at de-rated modes [15], [25]. The quantities for the offered IPFR are flexible. The thermal generator can only provide fixed level IPFR when it is online. Its inertia comes from the kinetic energy stored in the rotating parts, which can be expressed as H_i^{TH0}. The primary frequency response (PFR) is offered by governor control, which can be represented by $P_i^{\mathrm{G,PF0}}$. Therefore, the on/off status of thermal generators should be considered when determining the system IPFR quantities.

To depict the spot market in power systems with high VRE penetration, this paper considers the energy, IPFR, and reserve markets in the clearing process. A schematic diagram of the joint spot markets is shown in Fig. 1. First, participants need to provide two types of information. One is the bidding information, including step-wise curves for the energy market and single offers for ancillary markets. The other is operation characteristics, such as the minimum online time of thermal generators and the maximum energy capacity of ES. Next, based on the collected information, the system operator runs the joint clearing process to obtain the market clearing results, including market clearing prices and cleared quantities for participants.

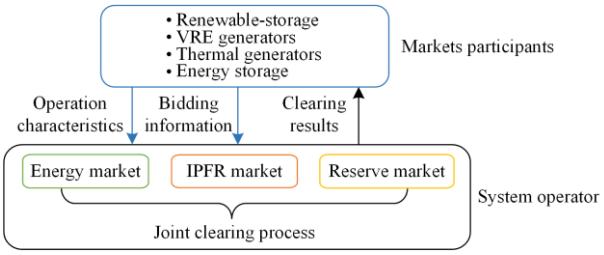

Fig. 1. Spot market schematic diagram.

B. Bi-level Model

To analyze the RSS bidding strategy in future spot markets as a price-maker, this paper proposes a bi-level model. The upper-level indicates the profits from multiple markets, including energy, IPFR and reserve. The lower-level simulates the market clearing process, in which the UC process is integrated to obtain the generators' on/off status. The framework for the proposed bi-level model is shown in Fig. 2.

The upper-level is the RSS bidding strategy problem, in which the profits from energy, IPFR and reserve markets are calculated. The lower-level represents the multiple markets clearing process. Considering the uncertainties of renewable units in RSS, multiple scenarios are developed. The constraints include market requirements, and participants' operation constraints. The characteristics of various types of participants are involved. In addition, the orange and blue arrows indicate the information interacted between bi-level models.

Therefore, the proposed bi-level model determines RSS optimal bidding strategy, which can be effectively adapted in diverse scenarios. Detailed information on the bi-level model can be found in Section III.

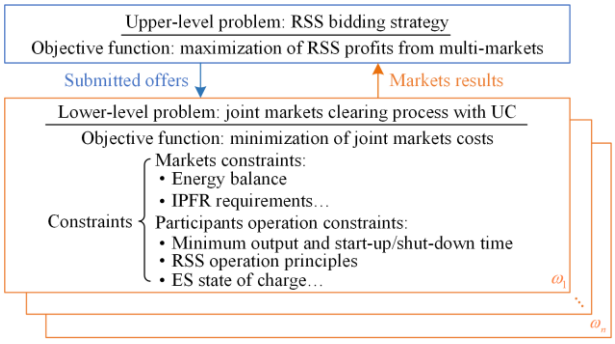

Fig. 2. Strategic bidding bi-level model framework.

III. Model Formulation

In this section, the upper-level model is proposed, which is the profit of the RSS earned from energy, IPFR, and reserve markets. Then, the lower-level model is built, which indicates the energy and ancillary markets clearing process with consideration of units' on/off status.

A. The Upper-level Model: Profit Maximalization

Considering the renewable units' uncertainties in RSS, the profit of RSS in multiple markets, can be expressed as:

$$R^{\mathrm{RSS}} = \max \sum_{\omega} \pi_{\omega} \left(R_{\omega}^{\mathrm{EN}} + R_{\omega}^{\mathrm{IPFR}} + R_{\omega}^{\mathrm{Re}} \right) \tag{1}$$

subject to:

$$\begin{aligned} R_{\omega}^{\mathrm{EN}} = & \sum_{i,t} \left(\lambda_{t,\omega}^{\mathrm{EN}} - C_i^{\mathrm{P,Op}} \right) \left(\sum_{b} P_{i,b,t,\omega}^{\mathrm{RSS,PEN}} \right) \Delta t - \\ & \sum_{t} \left(\lambda_{t,\omega}^{\mathrm{EN}} + C_i^{\mathrm{P,Op}} \right) \left(\sum_{b} P_{i,b,t,\omega}^{\mathrm{RSS,NEN}} \right) \Delta t \end{aligned} \tag{2}$$

$$\begin{aligned} R_{\omega}^{\mathrm{IPFR}} = & \sum_{t} \left(\lambda_{t,\omega}^{\mathrm{QSS\text{-}VI}} - C_i^{\mathrm{P,Op}} \right) P_{i,t,\omega}^{\mathrm{G,PF}} \Delta t + \\ & \sum_{t} \left(\lambda_{t,\omega}^{\mathrm{Sum\_H}} - C_i^{\mathrm{H,Op}} \right) H_{i,t,\omega}^{\mathrm{VI}} \Delta t \end{aligned} \tag{3}$$

$$R_{\omega}^{\mathrm{Re}} = \sum_{t} \left[\zeta_t P_{i,t,\omega}^{\mathrm{Re}} \left(\lambda_{t,\omega}^{\mathrm{EN}} - C_i^{\mathrm{P,Op}} \right) + \lambda_{t,\omega}^{\mathrm{Re}} P_{i,t,\omega}^{\mathrm{Re}} \right] \Delta t \tag{4}$$

$$\alpha_{i,b}^{\min} \leqslant \alpha_{i,b} \leqslant \alpha_{i,b}^{\max}, \forall b \tag{5}$$

$$\alpha_{i,b-1} \leqslant \alpha_{i,b}, \forall b \geqslant 2 \tag{6}$$

where $\lambda_{t,\omega}^{\mathrm{EN}}$ is the energy market price; $\lambda_{t,\omega}^{\mathrm{QSS\text{-}VI}}$ and $\lambda_{t,\omega}^{\mathrm{Sum\_H}}$ are PFR and inertia price, respectively; and $\lambda_{t,\omega}^{\mathrm{Re}}$ is the price in reserve market. Equation (1) calculates the RSS's total profits. Equation (2) expresses the RSS's profit from energy market, which contains the income in discharge mode and the expenses at the charge mode. Equation (3) calculates the profit from IPFR market. Equation (4) indicates the profits from reserve market, including the capacity revenue and the actual deployed capacity revenue. Equations (5)–(6) guarantee the offering prices in energy and ancillary markets are within the prescribed range and the increasing characteristic of the offering block.

B. The Lower-level Model: Joint Markets Clearing

In this section, the joint market clearing model is built, including energy IPFR, and reserve markets, while considering the ED and UC processes. The optimization objective of the lower-level model is to minimize the cost of power system in scenario ω, which can be described by:

$$C_{\omega}^{\mathrm{TO}} = \min \sum_{t} \left(C_{t,\omega}^{\mathrm{EN}} + C_{t,\omega}^{\mathrm{IPFR}} + C_{t,\omega}^{\mathrm{Re}} + C_{t,\omega}^{\mathrm{U\text{-}TO}} + C_{t,\omega}^{\mathrm{D\text{-}TO}} \right) \tag{7}$$

where

$$\begin{aligned} C_{t,\omega}^{\mathrm{EN}} = & \left(\sum_{i \in \Omega_{\mathrm{VRE/TH}},b} \alpha_{i,b,t}^{\mathrm{EN}} P_{i,b,t,\omega}^{\mathrm{G,EN}} \right) \Delta t + \left(\sum_{i \in \Omega_{\mathrm{es}},b} \alpha_{i,b,t}^{\mathrm{EN}} P_{i,b,t,,\omega}^{\mathrm{D,EN}} \right) \Delta t + \\ & \left(\sum_{i \in \Omega_{\mathrm{RSS}},b} \alpha_{i,b,t,,\omega}^{\mathrm{EN}} P_{i,b,t,\omega}^{\mathrm{RSS,PEN}} \right) \Delta t - \left(\sum_{i \in \Omega_{\mathrm{es}},b} \alpha_{i,b,t}^{\mathrm{C}} P_{i,b,t,,\omega}^{\mathrm{C,EN}} \right) \Delta t - \\ & \left(\sum_{i \in \Omega_{\mathrm{RSS}},b} \alpha_{i,b,t}^{\mathrm{C}} P_{i,b,t,\omega}^{\mathrm{RSS,NEN}} \right) \Delta t \end{aligned} \tag{8}$$

$$C_{t,\omega}^{\mathrm{IPFR}} = \left(\sum_{i \in \Omega_{\mathrm{VRE/es/RSS}}} \alpha_{i,t,\omega}^{\mathrm{IN}} H_{i,t,\omega}^{\mathrm{VI}} + \sum_{i \in \Omega_{\mathrm{VRE/es/RSS}}} \alpha_{i,t,\omega}^{\mathrm{PF}} P_{i,t,\omega}^{\mathrm{G,PF}} \right) \Delta t \tag{9}$$

$$C_{t,\omega}^{\mathrm{Re}} = \left(\sum_{i} \alpha_{i,t,\omega}^{\mathrm{Re}} P_{i,t,\omega}^{\mathrm{Re}} \right) \Delta t \tag{10}$$

$$C_{t,\omega}^{\mathrm{U\text{-}TO}} = \sum_{i \in \Omega_{\mathrm{TH}}} C_{i,t,\omega}^{\mathrm{U}} \tag{11}$$

$$C_{t,\omega}^{\mathrm{D\text{-}TO}} = \sum_{i \in \Omega_{\mathrm{TH}}} C_{i,t,\omega}^{\mathrm{D}} \tag{12}$$

Equation (7) shows the total cost of multiple markets. Equation (8) shows the cost of the energy market, whose first term indicates the costs of VRE and thermal generators participating in the energy market. The second and third items describe the costs of ES and RSS in the discharge mode, while the fourth and fifth items are the costs in the charge mode. Equations (9)–(10) show the costs from IPFR and reserve markets. Equations (11)–(12) show the start-up and shut-down costs of the thermal generators.

The lower-level constraints include the clearing constraints from the joint market (energy and ancillary services) and the operation constraints of various types of generators.

1) The Joint Market Clearing Constraints

The energy market constraint can be expressed as:

$$\begin{aligned} & \sum_{i \in \Omega_{\mathrm{VRE/TH}},b} P_{i,b,t,\omega}^{\mathrm{G,EN}} + \sum_{i \in \Omega_{\mathrm{RSS}},b} P_{i,b,t,\omega}^{\mathrm{RSS,PEN}} - \sum_{i \in \Omega_{\mathrm{RSS}},b} P_{i,b,t,\omega}^{\mathrm{RSS,NEN}} + \\ & \sum_{i \in \Omega_{\mathrm{es}},b} P_{i,b,t,\omega}^{\mathrm{D,EN}} - \sum_{i \in \Omega_{\mathrm{es}},b} P_{i,b,t,\omega}^{\mathrm{C,EN}} - D_{t,\omega} = 0 : \lambda_{t,\omega}^{\mathrm{EN}}, \forall t, \forall \omega \end{aligned} \tag{13}$$

The IPFR market constraints include limitations on rate of change of frequency (RoCoF), quasi-steady-state (QSS) frequency and nadir frequency [12].

$$H_{t,\omega}^{\mathrm{T0}} = \sum_{i \in \Omega_{\mathrm{es/VRE/RSS}}} H_{i,t,\omega}^{\mathrm{VI}} + \sum_{i \in \Omega_{\mathrm{TH}}} x_{i,t,\omega}^{\mathrm{TH}} H_i^{\mathrm{TH0}} : \lambda_{t,\omega}^{\mathrm{Sum\_H}}, \ \forall t, \forall \omega \tag{14}$$

$$H_{t,\omega}^{\mathrm{T0}} \geqslant \frac{\Delta D}{2 \left| F_{\mathrm{RoCoF\text{-}max}} \right|} : \lambda_{t,\omega}^{\mathrm{Rocof}}, \quad \forall t, \forall \omega \tag{15}$$

$$\Delta P_{t,\omega}^{\mathrm{TH,TO}} + \Delta P_{t,\omega}^{\mathrm{RE,TO}} \geqslant \Delta D : \lambda_{t,\omega}^{\mathrm{QSS\text{-}TO}}, \quad \forall t, \forall \omega \tag{16}$$

$$\Delta P_{t,\omega}^{\mathrm{TH,TO}} = \sum_{i \in \Omega_{\mathrm{TH}}} x_{i,t,\omega}^{\mathrm{TH}} P_i^{\mathrm{G,PF0}} : \lambda_{t,\omega}^{\mathrm{QSS\text{-}TH}}, \quad \forall t, \forall \omega \tag{17}$$

$$\Delta P_{t,\omega}^{\mathrm{VI,TO}} = \sum_{i \in \Omega_{\mathrm{VRE/es/RSS}}} P_{i,t,\omega}^{\mathrm{G,PF}} : \lambda_{t,\omega}^{\mathrm{QSS\text{-}VI}}, \quad \forall t, \forall \omega \tag{18}$$

$$\begin{aligned} & \left\| \begin{bmatrix} 1 & \dfrac{-\mathrm{T}_{\mathrm{PFR}}^{\mathrm{VI}}}{4\Delta f_{\max}} & \dfrac{-1}{T_{\mathrm{PFR}}^{\mathrm{TH}}} & 0 \\ 0 & \dfrac{-1}{\sqrt{\Delta f_{\max}}} & 0 & \dfrac{1}{\sqrt{\Delta f_{\max}}} \end{bmatrix} \begin{bmatrix} H_{t,\omega}^{\mathrm{T0}} \\ \Delta P_{t,\omega}^{\mathrm{VI,TO}} \\ \Delta P_{t,\omega}^{\mathrm{TH,TO}} \\ \Delta D \end{bmatrix} \right\| \leqslant \\ & \begin{bmatrix} 1 & \dfrac{-T_{\mathrm{PFR}}^{\mathrm{VI}}}{4\Delta f_{\max}} & \dfrac{1}{T_{\mathrm{PFR}}^{\mathrm{TH}}} & 0 \end{bmatrix} \times \\ & \begin{bmatrix} H_{t,\omega}^{\mathrm{T0}} \\ \Delta P_{t,\omega}^{\mathrm{VI,TO}} \\ \Delta P_{t,\omega}^{\mathrm{TH,TO}} \\ \Delta D \end{bmatrix} : \lambda_{t,\omega}^{\mathrm{Nadir\text{-}1}}, \lambda_{t,\omega}^{\mathrm{Nadir\text{-}2}}, \lambda_{t,\omega}^{\mathrm{Nadir\text{-}3}}, \quad \forall t, \forall \omega \end{aligned} \tag{19}$$

where $\lambda_{t,\omega}^{\text{Sum\_H}}$, $\lambda_{t,\omega}^{\text{Rocof}}$ $\lambda_{t,\omega}^{\text{QSS-TO}}$, $\lambda_{t,\omega}^{\text{QSS-TH}}$, $\lambda_{t,\omega}^{\text{QSS-VI}}$, $\lambda_{t,\omega}^{\text{Nadir-1}}$, $\lambda_{t,\omega}^{\text{Nadir-2}}$, and $\lambda_{t,\omega}^{\text{Nadir-3}}$ are the dual variables of corresponding constraints.

Constraints (14)–(15) indicate the system's total inertia should meet the requirement of RoCoF to avoid the disconnection of generators. Constraints (16)–(18) show the source of system's PFR and guarantee the adequacy of QSS frequency. Constraint (19) shows the nadir frequency constraints in rotated SOC form which can conveniently obtain the corresponding dual variables. The detailed derivation process can be found in [19].

Next, the reserve market clearing constraint can be expressed as:

$$\sum_i P_{i,t,\omega}^{\text{Re}} \geqslant P_{t,\omega}^{\text{Re-min}} : \lambda_{t,\omega}^{\text{Re}}, \quad \forall t, \forall \omega \tag{20}$$

where $\lambda_{t,\omega}^{\text{Re}}$ represents the system reserve requirement corresponding dual variable.

2) Market Cleared Quantities Constraints

$$P_{i,b,t}^{(\cdot),\text{EN}-\min} \leqslant P_{i,b,t,\omega}^{(\cdot),\text{EN}} \leqslant P_{i,b,t}^{(\cdot),\text{EN}-\max} : \mu_{i,b,t,w}^{(\cdot),\text{EN}-\max}, \mu_{i,b,t,w}^{(\cdot),\text{EN}-\min}, \quad \forall b, \forall t, \forall \omega \tag{21}$$

where $P_{i,b,t,\omega}^{(\cdot),\text{EN}}$ is the participants' cleared capacity in block b; $P_{i,b,t}^{(\cdot),\text{EN}-\min}$ and $P_{i,b,t}^{(\cdot),\text{EN}-\max}$ are the lower and upper cap of block b; $\mu_{i,b,t,w}^{(\cdot),\text{EN}-\max}$ and $\mu_{i,b,t,w}^{(\cdot),\text{EN}-\min}$ are the corresponding dual variables; and the superscript "(·)" can be "G", "D", "C", and "RSS" respectively.

Constraint (21) indicates the power output and discharge constraints for each block in energy market.

3) Market Participants' Operation Constraints

First, constraints (22)–(32) indicate the operation constraints for RSS based on its operation characteristics. Due to space limitations, the standalone ES operation constraints is not listed in detail, which is similar to the ES units in RSS [29].

Constraints (22)–(25) indicate the relationship between the RSS output and the output of renewable and ES units charge/discharge within RSS in energy, inertia, PFR and reserve markets, respectively.

$$\sum_b P_{i,b,t,\omega}^{\text{RSS,PEN}} - \sum_b P_{i,b,t,\omega}^{\text{RSS,NEN}} = P_{i,t,\omega}^{\text{W,EN}} + P_{i,t,\omega}^{\text{ESS,D}} - P_{i,b,t,\omega}^{\text{ESS,C}} : \mu_{i,t,w}^{\text{RSS,EN}}, \quad \forall i \in \Omega_{\text{RSS}}, \forall t, \forall \omega \tag{22}$$

$$P_{i,t,\omega}^{\text{G,IN}} = 2\left|F_{\text{RoCoF-max}}\right| H_{i,t,\omega}^{\text{VI}} = P_{i,t,\omega}^{\text{W,IN}} + P_{i,t,\omega}^{\text{ESS,IN}} : \mu_{i,t,w}^{\text{RSS,IN}}, \quad \forall i \in \Omega_{\text{RSS}}, \forall t, \forall \omega \tag{23}$$

$$P_{i,t,\omega}^{\text{G,PF}} = P_{i,t,\omega}^{\text{W,PF}} + P_{i,t,\omega}^{\text{ESS,PF}} : \mu_{i,t,w}^{\text{RSS,PF}}, \forall i \in \Omega_{\text{RSS}}, \forall t, \forall \omega \tag{24}$$

$$P_{i,t,\omega}^{\text{Re}} = P_{i,t,\omega}^{\text{W,Re}} + P_{i,t,\omega}^{\text{ESS,Re}} : \mu_{i,t,w}^{\text{RSS,Re}}, \forall i \in \Omega_{\text{RSS}}, \forall t, \forall \omega \tag{25}$$

Constraint (26) indicates the total VRE generator output should within its available capacity range.

$$P_{i,t,\omega}^{\text{W,EN}} + P_{i,t,\omega}^{\text{W,IN}} + P_{i,t,\omega}^{\text{W,PF}} + P_{i,t,\omega}^{\text{W,Re}} \leqslant P_{i,t,\omega}^{\text{WTMAX}} : \mu_{i,t,w}^{\text{W,TO}}, \forall i \in \Omega_{\text{RSS}}, \forall t, \forall \omega \tag{26}$$

Constraints (27)–(28) are used to limit the overall charge and discharge power of ES.

$$P_{i,t,\omega}^{\text{ESS,D}} + P_{i,t,\omega}^{\text{ESS,IN}} + P_{i,t,\omega}^{\text{ESS,PF}} + P_{i,t,\omega}^{\text{ESS,Re}} \leqslant P_{i,t,\omega}^{\text{DTMAX}} : \mu_{i,t,w}^{\text{D,TO}}, \forall i \in \Omega_{\text{RSS}}, \forall t, \forall \omega \tag{27}$$

$$P_{i,t,\omega}^{\text{ESS,C}} \leqslant P_{i,t,\omega}^{\text{CTMAX}} : \mu_{i,t,w}^{\text{C,TO}}, \quad \forall i \in \Omega_{\text{RSS}}, \forall t, \forall \omega \tag{28}$$

Constraint (29) limits the state of charge (SOC) range of ES in RSS and constraint (30) defines the SOC of ES at the beginning of the day.

$$E_{i,t,\omega}^{\text{EN}} \leqslant E_i^{\text{EN}_{\max}} : \mu_{i,t,w}^{\text{SOC-max}}, \quad \forall i \in \Omega_{\text{RSS}}, \forall t, \forall \omega \tag{29}$$

$$E_{i,t,\omega}^{\text{EN}} = E_i^{\text{Initial}} : \mu_{i,t,w}^{\text{SOCT}}, \quad \forall i \in \Omega_{\text{RSS}}, \; t = N_{\text{T}}, \forall \omega \tag{30}$$

Constraints (31)–(32) calculate ES's SOC at each end of the hour.

$$E_{i,t,\omega}^{\text{EN}} = E_{i,t-1,\omega}^{\text{EN}} + \left\{ \begin{matrix} P_{i,t,\omega}^{\text{ESS,C}} \eta_i - P_{i,t,\omega}^{\text{ESS,D}} / \eta_i - \\ \left(P_{i,t,\omega}^{\text{G,IN}} + P_{i,t,\omega}^{\text{G,PF}} + P_{i,t,\omega}^{\text{Re}} \right) \dfrac{\zeta_{t,\omega}}{\eta_i} \end{matrix} \right\} \Delta t : \mu_{i,t,w}^{\text{SOC}}, \quad \forall i \in \Omega_{\text{RSS}}, \forall t \geqslant 2, \forall \omega \tag{31}$$

$$E_{i,t,\omega}^{\text{EN}} = E_i^{\text{Initial}} + \left\{ P_{i,t,\omega}^{\text{ESS,C}} \eta_i - \left[\begin{matrix} \dfrac{P_{i,t,\omega}^{\text{ESS,D}}}{\eta_i} + \\ \left(\begin{matrix} P_{i,t,\omega}^{\text{G,IN}} + \\ P_{i,t,\omega}^{\text{G,PF}} + P_{i,t,\omega}^{\text{Re}} \end{matrix} \right) \dfrac{\zeta_{t,\omega}}{\eta_i} \end{matrix} \right] \right\} \Delta t : \mu_{i,t,w}^{\text{SOC}}, \quad \forall i \in \Omega_{\text{RSS}}, \; t = 1, \; \forall \omega \tag{32}$$

In addition, $\mu_{i,t,w}^{\text{RSS,EN}}$ $\mu_{i,t,w}^{\text{RSS,IN}}$ $\mu_{i,t,w}^{\text{RSS,PF}}$, $\mu_{i,t,w}^{\text{RSS,Re}}$, $\mu_{i,t,w}^{\text{W,TO}}$, $\mu_{i,t,w}^{\text{D,TO}}$, $\mu_{i,t,w}^{\text{C,TO}}$, $\mu_{i,t,w}^{\text{SOC-max}}$, $\mu_{i,t,w}^{\text{SOCT}}$, and $\mu_{i,t,w}^{\text{SOC}}$ are the dual variables for the corresponding constraints.

Then, the operation constraints for thermal generators can be expressed as:

$$\sum_b P_{i,b,t,\omega}^{\text{G,EN}} \geqslant x_{i,t,\omega} P_i^{\text{G,Min}} : \mu_{i,t,w}^{\text{GT}_{\min},\text{TO}}, \forall i \in \Omega_{\text{TH}}, \forall t, \forall \omega \tag{33}$$

$$\sum_b P_{i,b,t,\omega}^{\text{G,EN}} + P_{i,t,\omega}^{\text{Re}} \leqslant x_{i,t,\omega} P_i^{\text{G,Max}} : \mu_{i,t,w}^{\text{GT}_{\max},\text{TO}}, \quad \forall i \in \Omega_{\text{TH}}, \forall t, \forall \omega \tag{34}$$

$$-P_i^{\text{Ramp}} \leqslant \sum_b P_{i,b,t,\omega}^{\text{G,EN}} - \sum_b P_{i,b,t\text{-}1,\omega}^{\text{G,EN}} \leqslant P_i^{\text{Ramp}}, \quad \forall i \in \Omega_{\text{TH}}, \forall t \geqslant 2 : \mu_{i,t,w}^{\text{URamp}}, \mu_{i,t,w}^{\text{DRamp}} \tag{35}$$

$$C_{i,t,\omega}^{\text{U}} \geqslant 0 : \rho_{i,t,\omega}^{\text{U}}, \quad \forall i \in \Omega_{\text{TH}}, \forall t, \forall \omega \tag{36}$$

$$C_{i,t,\omega}^{\text{D}} \geqslant 0 : \rho_{i,t,\omega}^{\text{D}}, \quad \forall i \in \Omega_{\text{TH}}, \forall t, \forall \omega \tag{37}$$

$$C_{i,t,\omega}^{\text{U}} \geqslant (x_{i,t,\omega} - x_{i,t-1,\omega}) K_i^{\text{U}} : \sigma_{i,t,,\omega}^{\text{U}}, \quad \forall i \in \Omega_{\text{TH}}, \forall t, \forall \omega \tag{38}$$

$$C_{i,t,\omega}^{\text{D}} \geqslant (x_{i,t-1,\omega} - x_{i,t,\omega}) K_i^{\text{D}} : \sigma_{i,t,,\omega}^{\text{D}}, \quad \forall i \in \Omega_{\text{TH}}, \forall t, \forall \omega \tag{39}$$

$$-T_i^{\mathrm{U}}(x_{i,t,\omega}-x_{i,t-1,\omega})\geqslant-\sum_{r=t}^{t+T_i^{\mathrm{U}}-1}x_{i,r,\omega}:\phi_{i,t,\omega}^{\mathrm{U}},\quad \forall i\in\Omega_{\mathrm{TH}},\forall t=1,\cdots,N_{\mathrm{T}}-T_i^{\mathrm{U}}+1,\forall\omega \tag{40}$$

$$T_i^{\mathrm{D}}(x_{i,t,\omega}-x_{i,t-1,\omega})\geqslant-\sum_{r=t}^{t+T_i^{\mathrm{D}}-1}(1-x_{i,r,\omega}):\phi_{i,t,\omega}^{\mathrm{D}},\quad \forall i\in\Omega_{\mathrm{TH}},\forall\omega,\forall t=1,\cdots,N_{\mathrm{T}}-T_i^{\mathrm{D}}+1 \tag{41}$$

$$T_i^{\mathrm{D}}(x_{i,t,\omega}-x_{i,t-1,\omega})\geqslant-\sum_{r=t}^{t+T_i^{\mathrm{D}}-1}(1-x_{i,r,\omega}):\phi_{i,t,\omega}^{\mathrm{D}},\quad \forall i\in\Omega_{\mathrm{TH}},\forall\omega,\forall t=1,\cdots,N_{\mathrm{T}}-T_i^{\mathrm{D}}+1 \tag{42}$$

$$\sum_{r=t}^{N_{\mathrm{T}}}\left(1-x_{i,r,\omega}-\left(x_{i,t-1,\omega}-x_{i,t,\omega}\right)\right)\geqslant 0:\phi_{i,t,\omega}^{\mathrm{D}},\quad \forall i\in\Omega_{\mathrm{TH}},\forall t=N_{\mathrm{T}}-T_i^{\mathrm{D}}+2,\cdots,N_{\mathrm{T}},\forall\omega \tag{43}$$

$$x_{i,t,\omega}=\{0,1\},\ \forall i\in\Omega_{\mathrm{TH}},\forall t,\forall\omega \tag{44}$$

where $\mu_{i,t,w}^{\mathrm{GT_{min},TO}}$, $\mu_{i,t,w}^{\mathrm{GT_{max},TO}}$, $\mu_{i,t,w}^{\mathrm{URamp}}$, $\mu_{i,t,w}^{\mathrm{DRamp}}$, $\rho_{i,t,\omega}^{\mathrm{U}}$, $\rho_{i,t,\omega}^{\mathrm{D}}$, $\sigma_{i,t,,\omega}^{\mathrm{U}}$, $\sigma_{i,t,,\omega}^{\mathrm{D}}$, $\phi_{i,t,\omega}^{\mathrm{U}}$, and $\phi_{i,t,\omega}^{\mathrm{D}}$ are the dual variables for the corresponding constraints. Constraints (33)–(34) ensure the generator's output is within the acceptable range. Constraints (35), (36)–(39), and (40)–(43) represent the thermal generators' ramp up/down, start-up/shut-down, minimum up/down time constraints, respectively. Constraint (44) indicates that $x_{i,t,\omega}$ is a binary variable.

Next, the operation constraints for VRE units can be written as:

$$P_{i,t,\omega}^{\mathrm{G,Min}}\leqslant\sum_b P_{i,b,t,\omega}^{\mathrm{G,EN}}+P_{i,t,\omega}^{\mathrm{G,IN}}+P_{i,t,\omega}^{\mathrm{G,PF}}+P_{i,t,\omega}^{\mathrm{Re}}\leqslant P_{i,t,\omega}^{\mathrm{G,Max}}:\ \mu_{i,t,w}^{\mathrm{GT_{min},TO}},\mu_{i,t,w}^{\mathrm{GT_{max},TO}},\quad \forall i\in\Omega_{\mathrm{S/W}},\forall t,\forall\omega \tag{45}$$

$$P_{i,t,\omega}^{\mathrm{G,IN}}=2\left|F_{\mathrm{RoCoF-max}}\right|H_{i,t,\omega}^{\mathrm{VI}} \tag{46}$$

Constraint (45) indicates the overall power output in the energy and ancillary markets is within the range of available output power. Constraint (46) indicates the relationship between the inertia provided by VRE generator and the capacity reserved for inertia.

IV. Reformulation and Solution of Model

In this section, the solution method for the bi-level model developed in Section II is indicated. This process mainly includes three steps: reformulating of the lower-level model, transforming the bi-level model to a single level model, and addressing the non-linear items in the single level model.

A. Reformulation of the Lower-level Model

Based on [30], the reformulation of the lower-level model contains two steps.

First, by relaxing the binary variable ($x_{i,t,\omega}$) to continuous variables, the lower-level of the bi-level model built in Section II.B can be transferred to Model $\mathrm{B^C}$. The binary variables are relaxed as follows:

$$0\leqslant x_{i,t,\omega}\leqslant 1:\psi_{i,t,\omega}^{\min},\psi_{i,t,\omega}^{\max},\forall i\in\Omega_{\mathrm{th/VRE}},\forall t,\forall\omega \tag{47}$$

Constraint (47) shows the bounds for the relaxed binary variables.

Second, by adopting the dual theory, the dual from of Model $\mathrm{B^C}$ can be further derived, named as Model $\mathrm{B^*}$. Due to space limitation, the detailed dual form is not included. For clarity, the objective function and constraints in dual form are denoted as $B^{\mathrm{obj*}}$ and Constraints (dual), respectively.

Because of the relaxation of dual variables ($x_{i,t,\omega}$), the objective function values of Model B (expressed as B^{obj}) and Model $\mathrm{B^C}$ are not the same. According to the dual theory, at the optimal point, the objective function values of Model $\mathrm{B^C}$ and Model $\mathrm{B^*}$ (expressed as $B^{\mathrm{obj*}}$) are the same. Thus, B^{obj} and $B^{\mathrm{obj*}}$ are different, caused by the binary relaxation process. The difference between the values of B^{obj} and $B^{\mathrm{obj*}}$ among all scenarios can be denoted as D_{gap}, which can be calculated based on Equation (48). The smaller the D_{gap} value, the closer to the optimal point.

$$D_{\mathrm{gap}}=\sum_{\omega}(B_{\omega}^{\mathrm{obj}})-(B_{\omega}^{\mathrm{obj*}}) \tag{48}$$

B. Transfer Bi-level Model to Single Level Model

Based on the lower-level dual form (Model $\mathrm{B^*}$) and original lower-level model (Model B), this section transforms the original bi-level model to a single level model [31].

Through the penalty factor, the bi-level model can be reformulated to a single level problem as:

$$\max\left(R^{\mathrm{RSS}}-W\times D_{\mathrm{gap}}\right),\quad \text{s.t. } (2)-(6) \text{ and } (13)-(46) \tag{49}$$

where W is a factor that indicates the accuracy of the market clearing results between the original problem and the dual form lower-level problem. The original lower-level problem (including its objective function and constraints) remains in the reformulated single level problem.

C. Solve the Non-linear Items in Single Level Model

Although the bi-level has been transformed to a single level model, the presence of non-linear items in single level cannot be directly solved by the solver. Based on the binary expansion method [32], this section elaborates on the process for addressing non-linear items.

The non-linear items originate from two aspects. One is the calculation of income in markets in Eqs. (2)–(4). For instance, $\lambda_{t,\omega}^{\mathrm{EN}}P_{i,b,t,\omega}^{\mathrm{RSS,PEN}}$ indicates the RSS income in energy market. The other is the offered price of RSS

multiplied by the cleared capacity in multiple markets from Eqs. (8)–(10). For example, it can be found in energy market expressed as $\alpha^{\mathrm{EN}}_{i,b,t,,\omega} P^{\mathrm{G,EN}}_{i,b,t,,\omega}$. Considering the similarity in the treatment of these non-linear terms, $\lambda^{\mathrm{EN}}_{t,\omega} P^{\mathrm{RSS,PEN}}_{i,b,t,\omega}$ is selected as an example to demonstrate the process of handling nonlinearity.

First, $P^{\mathrm{RSS,PEN}}_{i,b,t,\omega}$ can be described as a set of discrete values $\{P^{\mathrm{RSS,PEN}}_{i,b,t,\omega,l}, l=1,2,\cdots,L\}$ with range $[0, P^{\mathrm{RSS,PEN\text{-}max}}_{i,b,t,\omega}]$ and can be expressed as:

$$P^{\mathrm{RSS,PEN}}_{i,b,t,\omega} = \sum_{m=0}^{\log\frac{L}{2}} 2^m \Delta_{i,b} y_{i,b,t,\omega,m}, \quad \forall i, \forall b, \forall t, \forall \omega \tag{50}$$

where $\Delta_{i,b} = P^{\mathrm{RSS,PEN\text{-}max}}_{i,b,t,\omega} \big/ (L-1)$ and $y_{i,b,t,\omega,m}$ is a binary variable.

Second, the non-linear item can be expressed as:

$$\lambda^{\mathrm{EN}}_{t,\omega} P^{\mathrm{RSS,PEN}}_{i,b,t,\omega} = \sum_m 2^m \Delta_{i,b} z_{i,b,t,\omega,m} \tag{51}$$

$$z_{i,b,t,\omega,m} = \lambda^{\mathrm{EN}}_{t,\omega} y_{i,b,t,\omega,m}, \quad \forall i, \forall b, \forall t, \forall \omega \tag{52}$$

where $\lambda^{\mathrm{EN}}_{t,\omega} P^{\mathrm{RSS,PEN}}_{i,b,t,\omega}$ can be replaced by the right-hand expression in (51), which is a linear term. Furthermore, the variable multiplication in (52) can be transferred to the constraints shown as:

$$0 \leqslant \lambda^{\mathrm{EN}}_{t,\omega} - z_{i,b,t,\omega,m} \leqslant M\left(1 - y_{i,b,t,\omega,m}\right), \forall m \tag{53}$$

$$0 \leqslant z_{i,b,t,\omega,m} \leqslant M \times y_{i,b,t,\omega,m}, \quad \forall m \tag{54}$$

where M is a large positive constant. When $y_{i,b,t,\omega,m} = 0$, constraint (54) is binding to ensure $z_{i,b,t,\omega,m}$ is zero. When $y_{i,b,t,\omega,m} = 1$, constraint (53) is binding and $z_{i,b,t,\omega,m}$ is equal to $\lambda^{\mathrm{EN}}_{t,\omega}$. Therefore, $\lambda^{\mathrm{EN}}_{t,\omega} P^{\mathrm{RSS,PEN}}_{i,b,t,\omega}$ can be replaced by $\sum_m 2^m \Delta_{i,b} z_{i,b,t,\omega,m}$ with constraints (54)–(53), which can be directly applied in solvers.

V. Numerical Examples

A. Basic Data

The numerical example is developed based on the IEEE30-bus system and the operation data from CAISO in 2019 are chosen to generate the available capacity of the VRE generators. There are four thermal generators, four PV stations, six wind-turbine stations, five ESs and one RSS. The bidding behavior of the RSS is represented by the combination of wind-turbines station and ES (WSS). The total installed capacity is set as 536 MW, in which thermal generators, PV stations, wind-turbine stations, ESs and WSS account for 15%, 35%, 30%, 6% and 14%, respectively. The costs of VRE and thermal generators are set as 6–10 \$/MWh and 30–40 \$/MWh, respectively, based on the data from [33], [34]. The inertia constant of thermal generators is 6 s, while the capability of thermal generators offering primary frequency response is set as 10% of their installed capacity [35]. The system disturbance is selected as 5% of the maximum daily demand. Referring to [18], RoCoF, nadir frequency and QSS frequency are set as 0.8 Hz/s, 49.5 Hz, and 49.7 Hz, respectively. Three scenarios are set when determining the RSS bidding strategy, S1, S2, and S3. The difference between the scenarios is reflected in the renewable unit available capacity in RSS. S2 is 1.1 times greater than S1, and S3 is 0.9 times of S1. The proposed illustrative example is implemented in modeling layer called YALMIP in MATLAB and solved by the commercial solver Gurobi.

It should be noticed that, the prices obtained from the single level model and calculated from original market clearing model with fixed RSS bidding prices and binary variables are not the same but are similar under all conditions. This is because of the relaxation of the binary variables in the solving process. Specifically, among the 72 price points considered (3 scenarios, 6 time periods and 4 markets), 42% of the prices from single level model and original market clearing model are the same, while 38% differ by less than 20%. Although the conversion between Model B and Model B* is not completely accurate, these two models are still close to each other and the prices generated from them are similar. Therefore, the lower-level model can effectively simulate the market clearing results, and the RSS strategic bidding behavior can be analyzed.

B. RSS Bidding Behaviors in Multi-market

The complicated bidding strategies of RSS in multiple markets can be analyzed by applying the model proposed in Section II. Figure 3 shows the clearing prices in energy, inertia, PFR and reserve markets and the RSS bidding prices in various scenarios. In each subplot, the solid lines indicate the market clearing price in various scenarios, and the dashed line is the RSS's offering price.

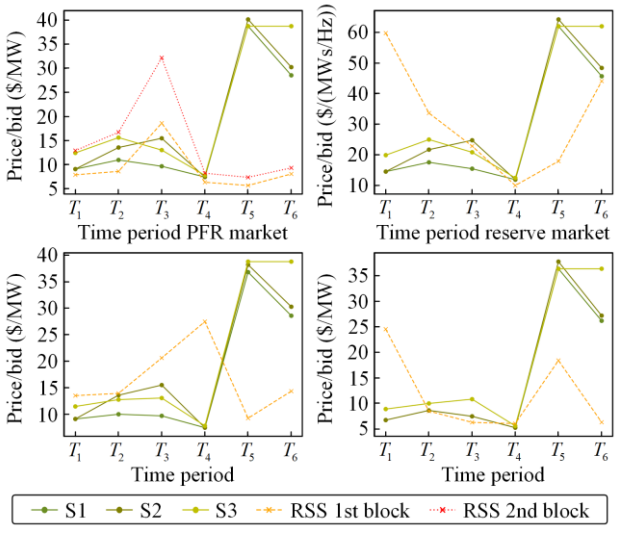

Fig. 3. Multi-market clearing prices and RSS bidding prices.

1) Bidding Strategies in Different Scenarios

In the energy market, when the clearing price reaches a higher level, particularly in T_5 and T_6, RSS strategically sets its offering prices in both blocks below the market's clearing price to enhance the volume of successfully cleared capacity. Conversely, at T_3, RSS strategically sets its offering prices in both blocks higher than the market's clearing price to avoid being cleared.

In addition, considering the wind power output uncertainty, the optimal bidding strategy seeks to maximize profit in different scenarios. When comparing the relationship between the market clearing price and the RSS offered price in different scenarios, different strategic behaviors can be found. In the inertia market at T_3, the bidding price is lower than that at S2 but higher than the clearing prices at S1 and S3. This means RSS chooses to be successfully cleared only in S2, because S2 has the maximum wind power output. At the same time, RSS participates only in the re-serve market in S1 and S3, and in the reserve and inertia markets in S2.

Therefore, by strategically adjusting the bidding price to financial withholding available capacity, RSS achieved clearance in higher price periods and scenarios.

2) Coordination of Bidding Behaviors in Multi-market

In energy market, the units are allowed to offer step-wise bidding curves with two blocks. During T_1 and T_2, the first block price offered by RSS is lower than the market clearing price, and the second block price is higher than the market clearing price. This means that RSS strategically withholds a segment of its capacity, ensuring that only a partial quantity of the total RSS capacity is cleared in the energy market. At T_1, the remaining RSS capacity is used to charge the storage in RSS. At T_3, RSS uses the residual capacity to participate in the inertia market in S2 and the reserve market in all scenarios. In addition, RSS intends to participate in partial markets by strategically offering prices. For instance, at T_1, RSS only participates in energy markets by offering higher value in other markets. At T_4, only in energy and inertia markets, RSS offers lower prices than the market clearing prices.

Based on the analysis of RSS bidding behavior in multiple markets, it can be concluded that RSS coordinates its bidding strategies across markets with two features. The first is the strategic withholding of a portion of capacity in the energy market to limit the cleared capacity. The second is selective participation across multiple markets by submitting higher bidding in certain markets to avoid being cleared.

C. Impacts on Market Clearing

This section explores the influence of RSS bidding behavior on the market clearing prices and its cleared capacities in multiple markets. The RSS strategic bidding behavior will change the type of markets and cleared capacities. The clearing results of T_2 in S3 are selected for further analysis, where the effects of strategic bidding are most pronounced. The case without RSS strategic bidding is named basic case (BC), shown as a blue curve, while the case with RSS strategic bidding is named strategic case (SC), shown as a green curve.

1) Comparison of Prices in BC and SC

Figure 4 illustrates the cumulative supply curve and WSS cleared quantity in multiple markets in the BC and SC. Figures 4(a)–(d) show the cumulative supply curves of energy, inertia, PFR and reserve market, respectively. The annotations for the market clearing price and WSS bidding information are also included.

In Fig. 4(a), at BC, the RSS bidding prices of the two blocks are both lower than the market clearing price. In SC, only the first block price offered by RSS is lower than the market price; this leads to strategic bidding behavior decreasing the amount of RSS cleared in the energy market, and the available capacity is saved for participating in other ancillary markets. In addition, compared with that of BC, the SC energy market price increased by 22.5%.

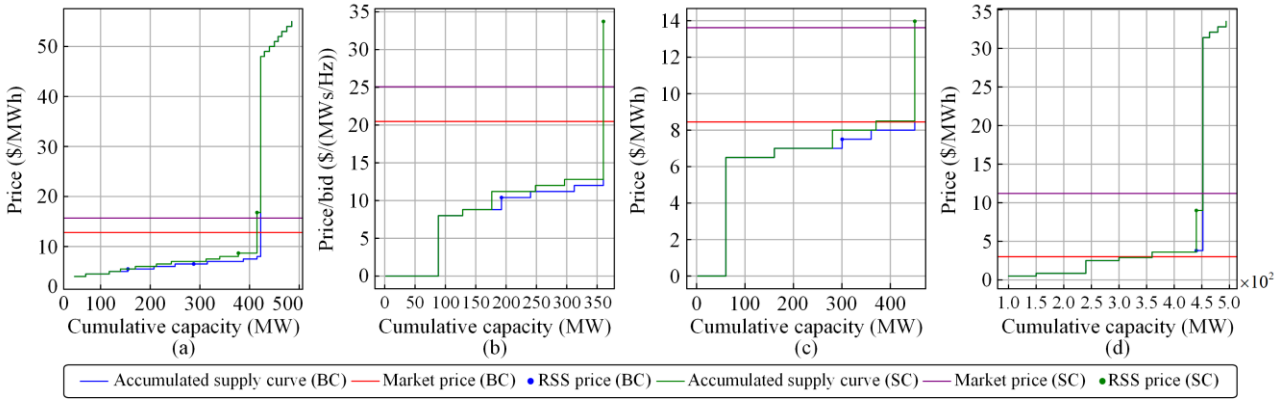

Fig. 4 Cumulative curves and RSS cleared capacity in multi-market at BC and SC. (a) Energy market cumulative curve. (b) Inertia market cumulative curve. (c) PFR market cumulative curve. (d) Reserve market cumulative curve.

In Fig. 4(b) and (c), the bidding strategies in the inertia and PFR markets are similar. The RSS bidding prices are lower than the corresponding market clearing price on BC and higher than the market clearing price in SC. This means that RSS tends to avoid being cleared in inertia and PFR markets and saves available capacity. Although RSS has not been cleared in inertia or the PFR market in SC, the inertia and the PFR market clearing price increase by 22.4% and 51.3%, respectively, compared with those of BC. In Fig. 4(d), the RSS bidding price is higher than the reserve market clearing price on BC and lower than market clearing price in SC. RSS is successfully cleared in SC in reserve market through strategic bidding behavior. The SC market price significantly increases and is twice that of the BC market.

2) Comparison RSS Cleared Capacity in BC and SC

TABLE I shows the RSS cleared capacity in BC and SC at T_2 in S3. Compared with that of BC, it can be found that the cleared capacity in energy market decreases in SC. The withhold capacity in the energy market is used to participate in the ancillary market. Besides, the number of markets in which RSS is cleared decreases. In BC, RSS is cleared in PFR and inertia markets. In SC, by increasing the offering in PFR and inertia market, RSS has only successfully been cleared in the reserve market. This results from the reserve market exhibiting a higher clearing price than the PFR and inertia markets. It can be concluded that, by strategically setting prices across multiple markets, RSS alters the cleared capacity in multiple markets and diminishes the number of markets that achieve clearance.

TABLE I
RSS CLEARED CAPACITY IN MULTI-MARKET

	Cleared capacity in markets (MW)			
	Energy	Inertia	PFR	Reserve
BC	18.50	1.56	1.86	0.00
SC	17.53	0.00	0.00	4.39

D. Influences of ES Installation

By comparing the situations with and without ES installation, this section indicates the effect of equipping ES with renewable units on its operation characteristics and system costs.

1) Influence of ES Installation on Renewable Units

To better demonstrate the influences of ES installation on a wind station, Table II shows the wind station operation status during the day in S1. In the table, "ES C" and "ES DC" indicate the equipped ES charge and discharge values, respectively. "RSS C" and "RSS DC" indicate the RSS overall charge and discharge power, respectively.

From the comparison of the power outputs of wind station with and without ES shown in Table II, it is observed that during T_3 and T_4, the output of wind station without energy storage is significantly lower than that of those equipped with ES. This discrepancy arises due to relatively high power output of renewable units during these two periods, leading to wind curtailment. During T_3 and T_4, the system VRE output is obviously higher than the demand and the equipped ES stores the surplus wind power. This enhances the wind power consumption capacity of the power system and the curtailed power of the wind station decreases by 18%.

Analyzing of the operation status of the wind station equipped with ES (RSS), reveals that ES stores surplus energy at T_1, T_3 and T_4, and releases energy mainly at T_5. Because the market clearing price has the highest value at T_5, ES significantly increases the revenue of the wind station. After being equipped with ES, the total profit of the wind station increases by 21.6%. Besides, RSS appears to be a generator rather than demand for the whole time. The SOC of RSS remains the same at the beginning and the end of the day, which conforms to real scenario.

Therefore, equipping renewable units with ES can mitigate the renewable energy curtailment phenomenon caused by the mismatch between new energy output and load demand. Furthermore, the revenue of the renewable units is also enhanced.

TABLE II
WIND STATION STATUS IN CASES WITH AND WITHOUT ES

		Time					
		1	2	3	4	5	6
Without ES	Wind output (MW)	21.6	15.1	6.1	9.3	22.2	24.1
With ES	Wind output (MW)	22.0	17.6	13.6	15.4	22.6	24.8
	ES DC (MW)	0.0	3.9	0.0	0.0	17.5	0.0
	ES C (MW)	16.8	0.0	8.8	3.4	0.0	0.70
	SOC (MWh)	29.6	21.1	26.2	40.0	19.4	20.0
	RSS C (MW)	0.0	0.0	0.0	0.0	0.0	0.0
	RSS DC (MW)	5.2	21.5	4.9	7.5	39.6	24.1

2) Influence of ES Installation on System Costs

In Fig. 5, the orange line indicates the system cost at BC with various percentages of ES in RSS. The system cost gradually decreases with increasing ES as the impact of VRE output violability during the day is diminished by ES. The blue line represents the system cost in SC with the same amount of ES. The difference between the BC and SC system costs shows a significant increase when the ES percentage in RSS is greater than 10%. This SC curve shifts from a declining to an ascending trend when the percentage exceeds 20%. This

means that the RSS bidding behavior has a significant influence on the market results and the potential market power may exist.

It can be concluded that, with the increase in the number of ES equipped with renewable stations, its strategic bidding strategies can strongly affect market clearing prices and further influence system costs. If the market clearing results are heavily affected by individual participants, this may lead to extra market power problems.

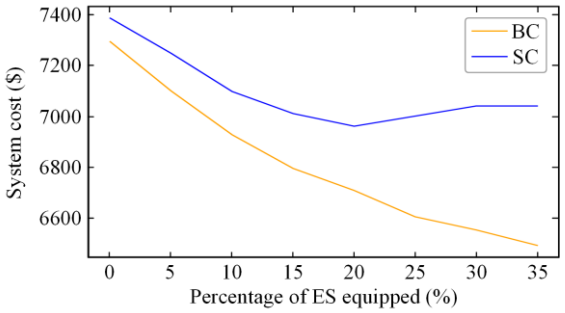

Fig. 5. System costs in BC and SC with various percentages of ES equipped.

VI. Conclusions

In power systems with high VRE penetration, corresponding markets have been designed in many studies to incentivize various types of participants to provide IPFR. With the increase in market types, the participants' bidding behavior becomes more complicated. This paper proposes a bi-level model considering energy, IPFR and reserve markets to model the strategic behaviors of RSS. The violability of renewable output influences traditional generators' on/off status over a day and the IPFR process is highly related to the on/off status of generators. Thus, the binary variables expressing the on/off status must be embedded. A solution method based on penalty function and dual theory is developed to solve the non-convex bi-level model. The proposed model and solution method are tested on a numerical example. The results show that the proposed model and solution method can be effectively used to analyze the complicated bidding behavior of RSS.

By analyzing the results of the built numerical examples, the following conclusions can be drawn:

1) To achieve higher profits, RSS strategically aims to be successfully cleared in partial markets and controls its cleared capacity in multiple markets through financial withholding of its capacity. With strategic behavior, RSS is only cleared in two markets, whereas it is cleared in all markets without strategic bidding;

2) The strategic behavior of RSS leads to a significant increase in market prices and system costs. Specifically, prices in the energy and PFR markets increase by 22.5% and 51.3%, respectively, due to the RSS strategic behaviors;

3) The influence of the RSS strategic behaviors on the system becomes more pronounced when the percentage of storage equipped with renewable energy exceeds 20%, potentially leading to market power problems;

4) Considering the influence of renewable units equipped with storage, it is suggested that system operators should establish corresponding supervision measures to prevent excessive growth in system costs caused by the RSS strategic behaviors.

Acknowledgment

Not applicable.

Authors' Contributions

Kexin Li: conceptualization, methodology, software, visualization, and writing-original draft. Hongye Guo: conceptualization, methodology, writing-review, and supervision. Cheng Feng: methodology and editing. Songtai Yu: writing-review and editing. Yong Tang: conceptualization, methodology, and supervision. All authors read and approved the final manuscript.

Funding

This work is supported by the SGCC Science and Technology Project "Cost Analysis, Market Bidding Mechanism Research and Validation of New Power System Transformation under a Diversified Value System" (No.1400-202357380A-2-3-XG).

Availability of Data and Materials

Not applicable.

Declarations

Competing interests: The authors declare that they have no known competing financial interests or personal relationships that could have appeared to influence the work reported in this article.

Authors' Information

Kexin Li received the B.S. degree in electrical engineering from North China Electric Power University in June 2018 and Ph.D. degrees in electrical engineering from Tsinghua University, Beijing, China, in 2024. She is currently working at the China Electric Power Research Institute. Her research interests include electricity market mechanism design and optimal bidding.

Hongye Guo received the B.S. and Ph.D. degrees in electrical engineering from Tsinghua University, Beijing, China, in 2015 and 2020, respectively. He is currently an associate professor with the Department of Electrical Engineering, Tsinghua University. His research interests include electricity market, demand-side

flexibility, and applications of artificial intelligence in power system.

Cheng Feng received the B.S. degree in Electrical Engineering from Huazhong University of Science and Technology in June 2019, and the Ph.D. degree in Electrical Engineering from Tsinghua University in June 2024. During February 2023 to August 2023, he was a visiting scholar in the Automatic Control Laboratory, ETH Zürich. He is now the Ezra postdoctoral associate at Cornell University. His research interests include power system flexibility and stability, and the application of AI in energy systems.

Songtai Yu received the B.S. degree and Ph.D. degree in electrical engineering from Tsinghua University, Beijing, China, in 2012 and 2017, respectively. He is currently working at the Beijing Power Exchange Center. His research interests include the market design of high-penetration renewable energy systems, electricity market mechanisms, and power system economics.

Yong Tang received the Ph.D. degree in China Electric Power Research Institute, Beijing, China, in 2002. His research interests include power system simulation analysis and stability control.

REFERENCES

[1] J. Wang, N. Xie, and C. Huang *et al.*, "Two-stage stochastic-robust model for the self-scheduling problem of an aggregator participating in energy and reserve markets," *Protection and Control of Modern Power Systems*, vol. 8, no. 3, pp. 1-20, Jul. 2023,

[2] J. Chen, J. Cheng, and W. Wang *et al.*, "Control strategy for a virtual synchronous generator using a multi-parameter cooperative adaptive method," *Power System Protection and Control*, vol. 52, no. 23, pp. 74-85, Dec. 2024. (in Chinese)

[3] International Energy Agency, (2022, Dec.) "Renewables 2022-analysis and forecast to 2027," IEA, Paris, France, [Online]. Available: https://iea.blob.core.windows.net/assets/ada7af90-e280-46c4-a577-df2e4fb44254/Renewables2022.pdf

[4] PJM Planning Division, (2022, May) "Grid of future: PJM's regional planning perspective," PJM, Audubon, USA, [Online]. Available: https://pjm. com/-/media/library/reports-notices/special-reports/2022/20220510-grid-of-the-future-pjms-regional-planning-perspective.ashx

[5] F. Milano, F. Dorfler, and G. Hug *et al.*, "Foundations and challenges of low-inertia systems (invited paper)," in *2018 Power Systems Computation Conference (PSCC)*, Dublin, Ireland, Jun. 2018, pp. 1-25.

[6] P. Tielens, P. Henneaux, and S. Cole *et al*., "Penetration of renewables and reduction of synchronous inertia in the European power system–analysis and solutions," *Luxembourg: Publications Office of the European Union*, 2020.

[7] Fingrid, (2024, Jun.) "Frequency containment reserves (FCR products)," Fingrid, Helsinki, Finland, [Online]. Available: https://www.fingrid.fi/en/electricity-market/reserves_and_balancing/frequency-containment-reserves/

[8] Fingrid, (2024, Jun.) "Fast frequency reserve (FFR)," Fingrid, Helsinki, Finland, [Online]. Available: https://www.fingrid.fi/en/electricity-market/reserves_and_balancing/fast-frequency-reserve/

[9] National Grid ESO, (2020, Jan.) "National grid ESO outline new approach to stability services in significant step forwards towards a zero-carbon electricity system," National Grid ESO, Warwick, UK, [Online]. Available: https://www.nationalgrideso.com/news/national-grid-eso-outline-new-approach-stability-services-significant-step-forwards-towards

[10] International Energy Agency, (2021, Dec.) "How rapidly will the global electricity storage market grow by 2026? –analysis," IEA, Paris, France, [Online]. Available: https://www.iea.org/articles/how-rapidly-will-the-global-electricity-storage-market-grow-by-2026

[11] Z. Yi, Z. Chen, and K. Yin *et al.*, "Sensing as the key to the safety and sustainability of new energy storage devices," *Protection and Control of Modern Power Systems*, vol. 8, no. 2, pp. 1-22, Apr. 2023

[12] A. Mey, P. Hutchins, and V. Linga, (2023, Jul.) "Battery storage in the United States: an update on market trends," U.S. Energy Information Administration, Washington, USA, [Online]. Available: https://www.eia.gov/analysis/studies/electricity/batterystorage/

[13] B.-I. Craciun, T. Kerekes, and D. Sera *et al.*, "Frequency support functions in large PV power plants with active power reserves," *IEEE Journal of Emerging and Selected Topics in Power Electronics*, vol. 2, no. 4, pp. 849-858, Dec. 2014.

[14] A. Fernández-Guillamón, E. Gómez-Lázaro, and E. Muljadi *et al.*, "Power systems with high renewable energy sources: a review of inertia and frequency control strategies over time," *Renewable and Sustainable Energy Reviews*, vol. 115, Nov. 2019.

[15] Q. Peng, Y. Yang, and T. Liu *et al.*, "Coordination of virtual inertia control and frequency damping in PV systems for optimal frequency support," *CPSS Transactions on Power Electronics and Applications*, vol. 5, no. 4, pp. 305-316, Dec. 2020.

[16] L. Badesa, F. Teng, and G. Strbac, "Simultaneous scheduling of multiple frequency services in stochastic unit commitment," *IEEE Transactions on Power Systems*, vol. 34, no. 5, pp. 3858-3868, Sep. 2019.

[17] Z. Chu, U. Markovic, and G. Hug *et al.*, "Towards optimal system scheduling with synthetic inertia provision from wind turbines," *IEEE Transactions on Power Systems*, vol. 35, no. 5, pp. 4056-4066, Sep. 2020.

[18] L. Badesa, F. Teng, and G. Strbac, "Pricing inertia and frequency response with diverse dynamics in an MISOCP formulation," *Applied Energy*, vol. 260, Dec. 2019.

[19] Z. Liang, R. Mieth, and Y. Dvorkin, "Inertia pricing in stochastic electricity markets," *IEEE Transactions on Power Systems*, vol. 38, no. 3, pp. 2071-2084, May 2023.

[20] L. Badesa, C. Matamala, and Y. Zhou *et al* "Assigning shadow prices to synthetic inertia and frequency response reserves from renewable energy sources," *IEEE Transactions on Sustainable Energy*, vol. 14, no. 1, pp. 12-26, Jan. 2023.

[21] K. Li, H. Guo, and X. Fang *et al*., "Market mechanism design of inertia and primary frequency response with consideration of energy market," *IEEE Transactions on Power Systems*, vol. 38, no. 6, pp. 5701-5713, Nov. 2023.

[22] D. Xiao, H. Chen, and W. Cai *et al.*, "Integrated risk measurement and control for stochastic energy trading of a wind storage system in electricity markets," *Protection and Control of Modern Power Systems*, vol. 8, no. 4, pp. 1-11, Oct. 2023.

[23] A. Attarha, N. Amjady, and S. Dehghan, "Affinely adjustable robust bidding strategy for a solar plant paired with a battery storage," *IEEE Transactions on Smart Grid*, vol. 10, no. 3, pp. 2629-2640, May 2019.

[24] Y. Xie, W. Guo, and Q. Wu *et al.*, "Robust MPC-based bidding strategy for wind storage systems in real-time energy and regulation markets," *International Journal of Electrical Power & Energy Systems*, vol. 124, Jan. 2021.

[25] R. A. Kordkheili, M. Pourakbari-Kasmaei, and M. Lehtonen, "Optimal bidding strategy for offshore wind farms equipped with energy storage in the electricity markets," in *2020 IEEE PES Innovative Smart Grid Technologies Europe (ISGT-Europe)*, The Hague, Netherlands, Oct. 2020, pp. 859-863.

[26] F. J. Heredia, M. D. Cuadrado, and C. Corchero, "On optimal participation in the electricity markets of wind power plants with battery energy storage systems," *Computers & Operations Research*, vol. 96, pp. 316-329, Aug. 2018.

[27] M. Khojasteh, P. Faria, and Z. Vale, "A robust model for aggregated bidding of energy storages and wind resources in the joint energy and reserve markets," *Energy*, vol. 238, Jan. 2022.

[28] H. Ding, P. Pinson, and Z. Hu *et al.*, "Optimal offering and operating strategy for a large wind-storage system as a price maker," *IEEE Transactions on Power Systems*, vol. 32, no. 6, pp. 4904-4913, Nov. 2017.

[29] G. He, Q. Chen, and C. Kang *et al.*, "Optimal bidding strategy of battery storage in power markets considering performance-based regulation and battery cycle life," *IEEE Transactions on Smart Grid*, vol. 7, no. 5, pp. 2359-2367, Sep. 2016.

[30] Y. Ye, D. Papadaskalopoulos, and J. Kazempour *et al.*, "Incorporating non-convex operating characteristics into bi-level optimization electricity market models," *IEEE Transactions on Power Systems*, vol. 35, no. 1, pp. 163-176, Jan. 2020.

[31] D. J. White and G. Anandalingam, "A penalty function approach for solving bi-level linear programs," *Journal of Global Optimization*, vol. 3, no. 4, pp. 397-419, Dec. 1993.

[32] L. A. Barroso, R. D. Carneiro, and S. Granville *et al.*, "Nash equilibrium in strategic bidding: a binary expansion approach," *IEEE Transactions on Power Systems*, vol. 21, no. 2, pp. 629-638, May 2006.

[33] H. Guo, Q. Chen, and Q. Xia *et al.*, "Modeling strategic behaviors of renewable energy with joint consideration on energy and tradable green certificate markets," *IEEE Transactions on Power Systems*, vol. 35, no. 3, pp. 1898-1910, May 2020.

[34] F. Ueckerdt, L. Hirth, and G. Luderer *et al.*, "System LCOE: what are the costs of variable renewables?" *Energy*, vol. 63, pp. 61-75, Dec. 2013.

[35] H. Li, Y. Qiao, and Z. Lu *et al.*, "Frequency-constrained stochastic planning towards a high renewable target considering frequency response support from wind power," *IEEE Transactions on Power Systems*, vol. 36, no. 5, pp. 4632-4644, Sep. 2021.